University of Bath

Alternative formats
If you require this document in an alternative format, please contact:
openaccess@bath.ac.uk

Online Muscle Activation Onset Detection Using Likelihood of Conditional Heteroskedasticity of Electromyography Signals

Yansong Wang, *Student Member, IEEE*, Nathan Routledge, Yanzheng Zhao, and Dingguo Zhang, *Senior Member, IEEE*

Abstract—Surface electromyography (sEMG) signals are crucial in developing human-machine interfaces, as they contain rich information about human neuromuscular activities. *Objective*: The real-time, accurate detection of muscle activation onset (MAO) is significant for EMG-triggered control strategies in embedded applications like prostheses and exoskeletons. *Methods*: This paper investigates sEMG signals using the generalized autoregressive conditional heteroskedasticity (GARCH) model, focusing on variance. A novel feature, the likelihood of conditional heteroskedasticity (LCH) extracted from the maximum likelihood estimation of GARCH parameters, is proposed. This feature effectively distinguishes signal from noise based on heteroskedasticity, allowing for the detection of MAO through the LCH feature and a basic threshold classifier. For online calculation, the model parameter estimation is simplified, enabling direct calculation of the LCH value using fixed parameters. *Results*: The proposed method was validated on two open-source datasets and demonstrated superior performance over existing methods. The mean absolute error of onset detection, compared with visual detection results, is approximately 65 ms under online conditions, showcasing high accuracy, universality, and noise insensitivity. *Conclusion*: The results indicate that the proposed method using the LCH feature from the GARCH model is highly effective for real-time detection of muscle activation onset in sEMG signals. *Significance*: This novel approach shows great potential and possibility for real-world applications, reflecting its superior performance in accuracy, universality, and insensitivity to noise.

Index Terms—**Change point detection, muscle activation onset, surface electromyography, human machine interface, generalized auto regressive conditional heteroskedasticity (GARCH)**

I. INTRODUCTION

Surface electromyography (sEMG) is a physiological electrical signal, measured non-invasively from the surface of the skin, that indicates the neuromuscular activation of the underlying muscle fibers [1]. A variety of information can be extracted or inferred from this signal, such as muscle activation, muscle strength, joint angle, joint stiffness, motor unit action potential, etc. [2]. Hence sEMG has been widely applied in research and clinical practice. In particular, the detection of muscle activation onset (MAO) is of crucial importance in medicine, sports science, rehabilitation, and in assistive applications, for example, in the diagnosis of neuromuscular disorders, examination of muscle activity pattern dysfunction, triggering of rehabilitation devices [3], and control of neuro-prostheses.

In terms of data processing, applications of sEMG can be divided into those utilizing retrospective, offline processing methods and those requiring real-time, online analysis. Offline processing of sEMG signals is mostly used for diagnosis or evaluation, and thus can exploit the use of powerful computing resources and the complete signal recording retrospectively, for analysis. However, online sEMG applications have critical real-time requirements in which a processing delay of more than 200 milliseconds is considered unacceptable [4]. Consequently, a notable challenge arises in online applications as subsequent data cannot be acquired in advance. Such a processing method or system is causal, and must act without the availability of future information. Therefore, online detection algorithms often lag the actual moment of muscle activation, which is referred to as the detection latency or accuracy of the algorithm. Many applications in the field of control require real-time processing methods for sEMG signals. For instance, sEMG-based interfaces have been utilized in prostheses, exoskeletons, manipulators, VR devices, remote control devices, teleoperations, medical equipment, biofeedback applications, etc. [5]–[8]. This fosters the development of intelligent devices that incorporate human-machine interfaces (HMI). This paper focuses on improving the accuracy of online MAO detection, which plays a crucial role in developing an HMI within the field of EMG-triggered control, as it can provide indication of human motion intentions.

Broadly speaking, online sEMG analysis is akin to the theoretical problem of signal change point detection which has been widely studied in statistics and financial fields. The first relative study dates back to the 1950s [9] for industrial quality control. The main concept from research progress in this area over the years can be summarized as detecting change points based on alterations of the mean, standard deviation, and trend

(slope or intercept) values of continuous or count variables [10].

In a recent review of offline change-point detection, the algorithm is classified according to three points: cost/objective functions, search methods, and constraints (the penalty for multiple change points) [11]. This methodology is more suitable to application on offline MAO detection of sEMG signals. Suviseshamuthu et al. [12] proposed a profile-likelihood-based method with a discrete Fibonacci search. Here, the objective function is the superposition of two sets of profile likelihood functions based on the activation segment and resting segment, and the search method is a discrete Fibonacci search. Alternatively, Selvan et al.[13] proposed a scree-plot-based method. In this case, the objective function is the summation of error from piecewise linear regression, and the search method is an exhaustive search. Another example is the classic method, cumulative sum (CUSUM)[9]. In its various derivations [14], the objective function is the cumulative sum of a relevant index, while the search method is commonly a threshold value.

The above studies are focused on offline change point detection, whereby the sequence segmentation is conducted after the completed acquisition of a whole signal trial, also known as a retrospective or posteriori method [11]. This paper looks to consider online detection methods classed as a preprocessor/feature combined with a classifier, similar to the concept of machine learning. To begin with, the sEMG signal is processed using an envelope operation to acquire the energy information. On application of low-pass filtering (LPF), the filtered signal can then be regarded as a feature, and online MAO detection can be realized through use of a threshold classifier [15]. The Teager-Kaiser energy operator (TKEO) [16] is a wildly used non-linear filter for highlighting the muscle activations from the background noise in a raw sEMG signal. Such a preprocessing stage has also been utilized with a classifier, e.g. double threshold [17], and Bayesian changepoint detection [18], to achieve online MAO detection in the last century. An extended version of TKEO (ETKEO) has since been proposed, with a more general formula and powerful performance. Wavelet transforms (WT) are another common signal preprocessing method. Using these foundations, together with the application of a likelihood-based test statistic method as a classifier, provides an alternative MAO detection methodology [19]. A machine-learning-based method can also be used to approach the MAO detection problem. Liu et al. [20] used a sequential Gaussian mixture model (GMM) to classify the logarithmic power of EMG signals. Nardo et al. [21] developed a neural network with an input of an EMG feature set. Trigili et al. [22] developed a method for MAO detection using subject-independent, time-domain EMG features and GMM classifiers.

Consideration of these methods from the perspective of their interpretability, detection latency, and universality properties, these existing mainstream methods all have certain disadvantages: ETKEO is equivalent to filtering, and additional operation is required for MAO detection to lose timeliness; the WT is more appropriate for offline applications; LPF produces delays and is ineffective in magnifying the differential between the signal and noise;

machine learning lacks interpretability; the distribution of statistical methods related to data distribution may vary depending on different muscles or subjects. Unlike most previous studies that analyze signal amplitude in either the time or frequency domains, this paper focuses on examining the variance of the signal, specifically its heteroskedasticity. In 1982 [23], Engle proposed the autoregressive conditional heteroskedasticity (ARCH) model to analyze inflation and was awarded the Nobel Prize in Economic Sciences in 2003 for this contribution. Later, Rasool et al. [24] extracted the conditional heteroskedasticity from sEMG signals and realized the muscle activation segmentation based on the generalized ARCH (GARCH) model. Furthermore, Rasool et al. [25] realized the application of parameters of the GARCH model for enabling gesture classification.

Guided by these preceding ideas and foundations in signal variance analysis, this research investigated conditional heteroskedasticity in sEMG signals. Consequently, a simplified model with fixed parameters is proposed to accelerate the computational calculations. Furthermore, the likelihood of conditional heteroskedasticity (LCH), extracted from the GARCH model, is proposed as a novel feature for MAO detection in online applications. Experimental verification has shown that this method has lower detection delay and is independent of subject and muscle. It also exhibited a strong ability to suppress noise.

The remainder of this article is organized as follows: Section II details the analysis of the sEMG signal using the autoregressive and GARCH model, whereby the order of model which reflects heteroskedasticity is determined. Section III proposes the LCH feature and derives the calculation formulae in detail. In Section IV, the proposed features and MAO detection framework are verified on open-source datasets, and a horizontal comparison is made. This comparison between various methods is also performed to establish the efficacy of the proposed technique. Section V provides a discussion of the research, and a summarizing conclusion is presented in Section VI.

II. ANALYSIS OF SEMG SIGNALS BY ARIMA-GARCH MODEL

As a seemingly random time series, sEMG signals are typically analyzed by an autoregressive integrated moving average model (ARIMA). To develop a method to distinguish between resting states and motion states, sEMG signals of these two conditions were modeled by ARMIA analysis, and their similarities and differences were compared. Two sEMG signal trials were randomly selected as cases to analyze. A window length of 200 ms was selected, a value which corresponds to most situations within the sEMG-based interface. The relevant formulae of specific hypothesis testing methods and evaluation indexes are generally recognized and, therefore, will not be included here.

The ARIMA model can be simplified as autoregressive moving average model (ARMA) model if the time series is stable, therefore, the initial step was to assess the stability of the original sEMG signals: the Augmented Dickey-Fuller (ADF) test was utilized for this purpose. When evaluating for both the resting and motion states, the ADF results showed
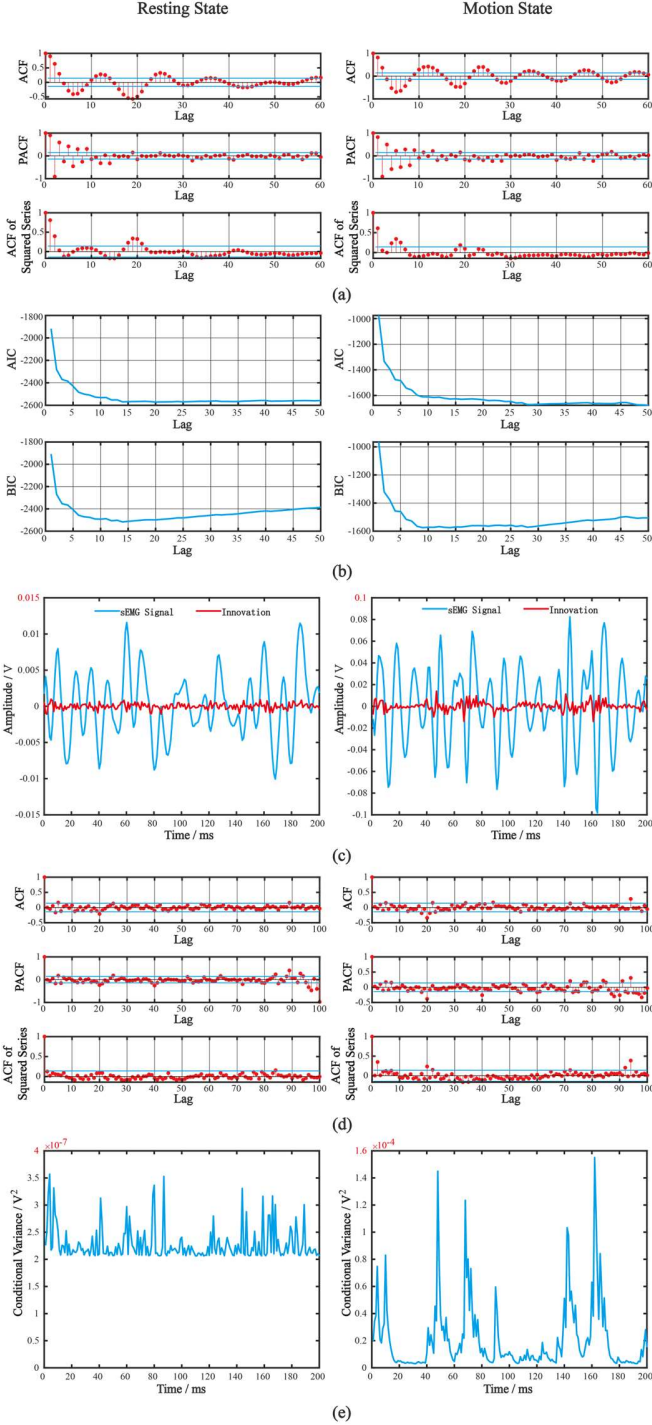
Fig. 1. The process of establishing the ARIMA-ARCH model. The left column is a segment of sEMG signal in the resting state, while the right column is in the motion state. (a) ACF and PACF analysis on raw signals. (b) AIC and BIC analysis for the determination of model order. (c) Raw sEMG signal segments and innovation of the AR model. (d) ACF and PACF analysis on the innovation. (e) Conditional variance reflecting heteroskedasticity.

that the testing could not reject the original hypothesis, hence both signals were considered stable. Therefore, the ARMA model was taken forward for modeling. Specific orders of the ARMA model were then determined based on the autocorrelation function (ACF) and partial autocorrelation function (PACF) of the signal segment, and the ACF of the squared signal segment. The results of the process on the

squared signal characterize the high-order autocorrelation. For details on the specific analysis criteria, refer to [26].

Fig. 1a presents the results of the ACF and PACF analysis, where the truncation and exponential attenuation emerge to a certain extent. The ARMA model can be further simplified to an autoregressive (AR) model. The absolute value of the ACF and PACF being greater than the blue threshold lines is considered significant. As a supplement to the ACF and PACF functions, the AR model order can be further determined with the use of the Akaike information criterion (AIC) and Bayesian information criterion (BIC), which are shown in Fig. 1b.

Considering it for use in online applications, specifically the online parameter identification of AR models, the order should, therefore, be kept as small as possible. Based on the described analysis, and results shown in Fig. 1a and Fig. 1b, a 10-order AR model was established as a unified model of sEMG signals in both the resting and motion states. All the model coefficients were determined as being significant, as verified using the MATLAB Econometrics Toolbox. Although this approach may not be extremely accurate, this verification method was deemed suitable for the task objectives, and appropriate for the subsequent analysis of heteroskedasticity. The original signals (in blue) and fitting residuals, or named innovations (in red), of the 10-order AR model are shown in Fig. 1c. Note the difference in the order of magnitude in the vertical axis between resting (left) and motion states (right).

Much of the previous research simply considers the signal amplitude when modeling an sEMG signal, and so settles with the AR model processing technique. However, the non-stationary sEMG signal is indicative of heteroskedastic properties. The ARCH model can simulate the volatility of a series. It determines the autoregressive order based on the innovations, using a process similar to that described above. The sequence initially needs to be tested for stationarity, and then by a Lagrange multiplier (LM) test to determine whether there is an ARCH effect. The ACF, PACF, and Ljung-Box (LB) test results demonstrated that the innovation of sEMG signals in the resting state could be regarded as white noise, while sEMG signals in the motion state showed an ARCH effect with a relatively higher order. Fig. 1d illustrates that the higher order autocorrelation of the innovation of the signal was stronger in the motion state. For example, in the 20th order, the ACF and PACF results in the motion state were still significant.

Four randomly selected sEMG signal trials (see Section III for further details on the dataset used) were modeled and analyzed. The corresponding innovation for a segment representing the motion state, and related statistical results are shown in Fig. 2. For each signal example, the plots shown, from the top-down, are the innovation, histogram, and Quantile-Quantile (QQ) plots, respectively. Based on this graphical verification, the innovation of sEMG signals modeled by the AR(10) model satisfied the hypothesis that the ARCH model assumes that the innovation is white noise.

For simulating the innovation of the AR model, a high-order ARCH model can be established based on the previously described analysis. However, the GARCH model, which can effectively fit a heteroskedasticity function with long-term autocorrelation, is proposed based on the same reasoning for

the ARCH model, while also effectively reducing the model order. Thus, a GARCH(1,1) model was adopted to model the innovation of sEMG signals in this research.

The heteroskedasticity of the signals is shown in Fig. 1e. A difference in the order of magnitude on the vertical axis is highlighted in red. This amplitude difference emphasizes that the resting state and the motion state were homoskedastic and heteroskedastic, respectively.

To this point, a method for the statistical modeling of surface EMG signals has been described: that is, a general model in the form of an AR(10)-GARCH (1,1) model. It should be emphasized that, in the resting state of signals, the parameters of the GARCH model may show no significance. In other words, the model is completely arbitrary. This difference is the basis for the subsequent classification between the motion and resting states.
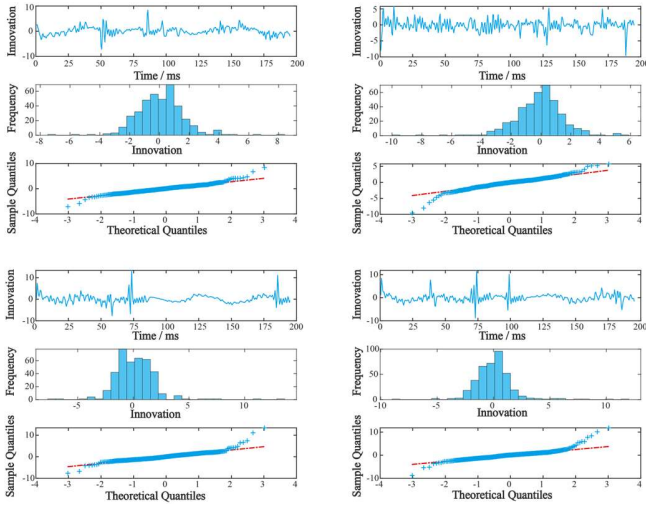

Fig. 2. Examples of test of normality for the innovations of an AR10 model on sEMG signals in the motion state.

III. FORMULA DERIVATION AND LCH FEATURE

It was observed that the heteroskedasticity model of the sEMG signals in the resting state differed from that in the motion state. Accordingly, an MAO detection scheme was proposed based on this phenomenon. This section goes on to describe the methods and associated formula derivations in detail.

A. Parameter Solving

This sub-section introduces the model and corresponding parameter identification method. All vectors are notated in bold text for differentiation, $x_n, n = [1,2, \dots, N]$ is the windowed sEMG signals and N is the window length. The offset of the average value is removed from the signals in each window. Thus, the general AR-GARCH model can be expressed as:

$$
\begin{aligned}
Y &= XA + \varepsilon \\
\varepsilon_t &= \sigma_t e_t \\
\sigma_t{}^2 &= \gamma + \sum_{p=1}^{m} \alpha_p \varepsilon_{t-p}{}^2 + \sum_{q=1}^{n} \beta_q \sigma_{t-q}{}^2
\end{aligned}
\tag{1}
$$

where A is coefficient vector composed of p-order AR model

coefficients a_p; ε_t is innovation trace; σ_t is the time-varying conditional variance of ε_t; α_p and β_q are the m-order and n-order regression coefficients of GARCH(m, n) ; γ is an offset parameter in GARCH model;

$$
\begin{aligned}
Y &= [x_{p+1}, x_{p+2}, \dots, x_N]' \\
X &= \begin{bmatrix} x_p & x_{p-1} & \cdots & x_1 \\ x_{p+1} & x_p & \cdots & x_2 \\ \vdots & \vdots & & \vdots \\ x_{N-1} & x_{N-2} & \cdots & x_{N-p} \end{bmatrix}' \\
A &= [a_0, a_1, \dots, a_p]' \\
\varepsilon &= [\varepsilon_{p+1}, \varepsilon_{p+2}, \dots, \varepsilon_N]'
\end{aligned}
\tag{2}
$$

and

$$
e_t \sim N(0, 1) \tag{3}
$$

is white noise.

Considering the analysis described in Section II, the following values were used in this study: p = 10, m = 1, n = 1, and $t = [11, 12, \dots, N]$.

In AR models, the least squares method is often used for online parameter identification, which is defined as $\hat{A} = (X'X)^{-1}X'Y$ where hatted symbols represent an estimated value. After substituting 'A' into equation (1) to get ε, then the GARCH(1,1) model may be established on the ε_t sequence.

The parameter set to be identified is $\theta_0 = \{\gamma, \ \alpha_0, \ \beta_0\}$. The residual can be simplified by recursion:

$$
\begin{aligned}
\sigma_t{}^2 &= \gamma + \alpha_0 \varepsilon_{t-1}{}^2 + \beta_0 \sigma_{t-1}{}^2 \\
&= \gamma + \alpha_0 \varepsilon_{t-1}{}^2 + \beta_0 (\gamma + \alpha_0 \varepsilon_{t-2}{}^2 + \beta_0 \sigma_{t-2}{}^2) \\
&= \gamma(1 + \beta_0) + \alpha_0 (\varepsilon_{t-1}{}^2 + \beta_0 \varepsilon_{t-2}{}^2) + \beta_0{}^2 \sigma_{t-2}{}^2 \\
&= \dots \dots \\
&= \gamma(1 + \beta_0 + \dots + \beta_0{}^{t-2}) + \alpha_0(\varepsilon_{t-1}{}^2 + \beta_0 \varepsilon_{t-2}{}^2 + \dots \\
&\quad + \beta_0{}^{t-2}\varepsilon_1{}^2) + \beta_0{}^{t-1}\sigma_1{}^2
\end{aligned}
\tag{4}
$$

According to the constraints that $\beta_0 \in [0,1)$ and the properties of series expansion, it can be derived that:

$$
\sigma_t{}^2 = \frac{\gamma}{1 - \beta_0} + \alpha_0 \sum_{j=1}^{t-1} \{\beta_0{}^{j-1} \varepsilon_{t-j}{}^2\} \tag{5}
$$

Let $V_t(\theta) = \sigma_t{}^2$ representing the function of conditional variance. On the other hand, $\sigma_t = V_t{}^{1/2}(\theta)$, so that:

$$
\varepsilon_t = V_t{}^{1/2}(\theta)e_t \tag{6}
$$

According to (3), and denoting the probability density function as f, then:

$$
\begin{aligned}
\int f(e_t)\, \mathrm{d}e_t &= 1 \\
\int V_t{}^{-1/2}(\theta)f(\varepsilon_t V_t{}^{-\frac{1}{2}}(\theta))\, \mathrm{d}\varepsilon_t &= 1
\end{aligned}
\tag{7}
$$

Equation (7) indicates that, for ε_t, its conditional probability density when observing information before t-1 is $V_t{}^{-\frac{1}{2}}(\theta)f(\varepsilon_t V_t{}^{-\frac{1}{2}}(\theta))$. The conditional probability density function is equal to the likelihood function in value, which is recorded as L, so the log likelihood function is:

$$
\ln L = \sum_{t=11}^{N} \ln \left[V_t{}^{-\frac{1}{2}}(\theta)f\left(\varepsilon_t V_t{}^{-\frac{1}{2}}(\theta)\right) \right] \tag{8}
$$

$$= \sum_{t=11}^{N} -\left[\frac{1}{2}\ln V_t - \ln f\left(\varepsilon_t V_t^{-\frac{1}{2}}\right)\right]$$

The gradient of the objective function is used in the optimization algorithm. Thus, the derivative of (8) is:

$$-\frac{d\ln L}{d\theta} = \sum_{t=11}^{N}\left[\frac{1}{2}\frac{V_t'}{V_t} - \frac{f'(\varepsilon_t V_t^{-\frac{1}{2}})}{f(\varepsilon_t V_t^{-\frac{1}{2}})} - \frac{1}{2}\varepsilon_t V_t^{-\frac{3}{2}}V_t'\right]$$

$$= \sum_{t=1}^{N}\frac{1}{2}\left\{\frac{V_t'}{V_t}\left[1 + \varepsilon_t V_t^{-\frac{1}{2}}\frac{f'(\varepsilon_t V_t^{-\frac{1}{2}})}{f(\varepsilon_t V_t^{-\frac{1}{2}})}\right]\right\} \quad (9)$$

$$= \sum_{t=11}^{N}\frac{1}{2}\left\{1 - H\left[\varepsilon_t/V_t^{\frac{1}{2}}(\theta)\right]\right\}\frac{V_t'(\theta)}{V_t(\theta)}$$

where

$$V_t'(\theta) = \left[\frac{1}{1-\beta_0}, \sum_{j=1}^{t-1}\{\beta_0^{j-1}X_{t-j}^2\}, \frac{\gamma}{(1-\beta_0)^2} + \alpha_0\sum_{j=1}^{t-1}\{(j-1)\beta_0^{j-2}X_{t-j}^2\}\right]' \quad (10)$$

$$H[x] = x(-\frac{f'(x)}{f(x)}) \quad (11)$$

H is the 'score function' for the M-estimation in the scale model [27]. According to the M-estimation theory, the quasi-MLE estimation is realized when setting $H[x] = x^2$, and so the calculation can be simplified.

The maximum likelihood method can be realized to estimate the parameters with (8) and (9). A sequential quadratic programming (SQP) algorithm may be adopted as a solver here to ensure the possibility of online calculation.

According to the assumptions, f conforms to a standard Gaussian distribution, which was verified by the results of the statistical testing presented in Fig. 2. Therefore, (8) can be further reduced to:

$$\ln L = \sum_{t=11}^{N} -\left[\frac{1}{2}\ln(\sigma_t^2) + \frac{1}{2}\frac{\varepsilon_t^2}{\sigma_t^2} + \ln(2\pi)\right] \quad (12)$$

The log-likelihood value can then be calculated within each window according to (12). So far, the model parameters $\widehat{\theta_0}$ can be estimated online via a maximum likelihood estimation within each window.

B. Feature and Classifier

According to the previously described analysis, an sEMG signal in the motion state has observable heteroskedasticity, in comparison with the resting state which tends towards homoskedasticity. Based on the assumption of the GARCH model, both ε_t and e_t comply with a standard normal distribution. Thus, the sEMG signals corresponding to a muscle's motion state would be directly reflected in the signal heteroskedasticity. As such, when the variance shows heteroskedasticity, to meet the distribution assumption of ε_t, the distribution of e_t will inevitably be affected. Specifically, in the motion state, the parameters of the GARCH model should have a lower likelihood value, lower logarithmic likelihood value, and larger LCH value. Therefore, the LCH value was proposed as a feature for detecting muscle activation. This value would reflect two relatively stable

modes, representing the motion state and the rest state, with different amplitudes. When the muscle activation state changes, the LCH value will gradually change from one stable state to another, demonstrating a 'bistable' characteristic. The specific calculation formula of the LCH is (13), being a simplification of Eq. (12), as follows:

$$LCH = \sum_{t=11}^{N}\left[\ln(\sigma_t^2) + \varepsilon_t^2/\sigma_t^2\right] \quad (13)$$

Because it is a one-dimensional scalar value, only threshold (OT) classifiers may be utilized to detect the instance of muscle activation. A basic OT classifier is commonly described as:

$$Th = \mu_{baseline} + k * \sigma_{baseline} \quad (14)$$

where k is the multiplier, typically with a value ranging from 3 to 15, which affects the sensitivity. The values μ and σ represent the mean and variance, respectively, which need to be initialized. It is recommended to use signal samples within the initial few windows after the system is powered on, which can be considered as being in a resting state. The corresponding flowchart of this method is shown in Fig. 3. The step of the sliding window should be as small as feasible, such as selecting a single sample, to facilitate the timely update of LCH features.
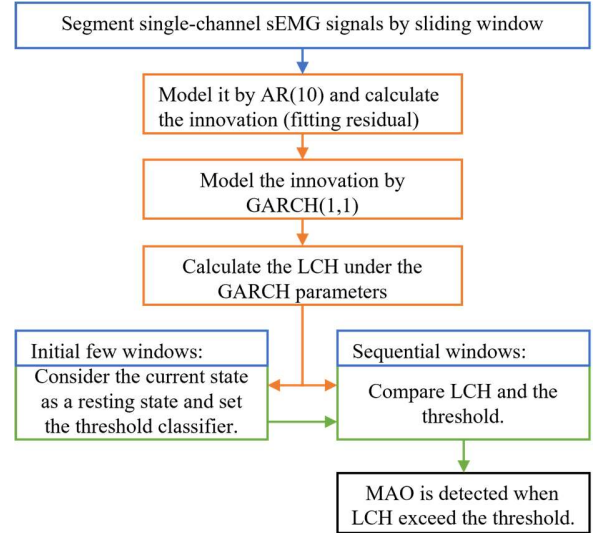

Fig. 3. Flowchart of the proposed MAO detection framework.

C. Model Simplification for Online Calculation

Online parameter identification of $\widehat{\theta_0}$ poses a computational challenge to real-time detection of muscle activation and, in some cases, may not converge to the global optimal solution. For that reason, this section describes the investigation of fixed $\widehat{\theta_0}$ parameters, rather than the use of online parameter optimization. From the perspective of MAO detection, the accuracy of the $\widehat{\theta_0}$ estimation is insignificant as it merely forms an intermediate step.

The GARCH(1,1) model has three parameters, where the first, γ, can be considered as an offset. In this paper, the innovation is considered as white Gaussian noise, and its offset bias can be approximately assumed as zero, therefore, γ is fixed as zero for simplicity.

Subsequently, the relationship between the parameters and

LCH characteristics was explored to find the internal rules for simplifying the parameter identification. For the two example signal segments presented in Fig. 1, the LCH values were calculated using a range of possible α_0 and β_0 parameter values, the results of which are shown in a mesh plot and contour subplot in Fig. 4. The x-axis and y-axis give the values of the parameters α_0 and β_0, ranging from 0 to 1, and the z-axis shows the LCH value. The LCH value has no unit, and the absolute value of the amplitude has no explicit meaning, and therefore only reflects information when under direct comparison. The mesh plots in the first row (Fig. 4a) show a global perspective, indicating that if the two parameters of the GARCH model were set to zero, there would be a large scope for optimization of the likelihood value. The remaining region of the parameter space shown in Fig. 4a, tended to be flat at this scale. The second row of plots (Fig. 4b) show a local enlargement, examining the regions near the extreme value. The macroscopic flat region had a clearer gradient when enlarged, suggesting the availability of a global optimal solution. Fig. 4c provides two-dimensional plots from the top view, with only the LCH values near the extreme point being retained. It was found that the position on the approximate diagonal line reached the extreme value, and the gradient in this direction was very small. LCH values in the motion and rest states reflected similar changes, and reached the extremum at close locations. Therefore, the α and β were manually fixed to values of 0.1 and 0.9, avoiding online parameter iterative optimization which, thereby, saves on

computational calculation efforts. For brevity, the use of fixed GARCH(1,1) model parameters to calculate the LCH value sequence will hereafter be referred to as LCH, while the method that requires online optimization shall be noted as LCH-Opt.

This analysis was performed based only on the two examples mentioned previously. Therefore, having fixed the parameters based on this analysis, irregularities in the signal may lead to sudden changes in the LCH value, which may pose as noise when performing classification through an OT method. Hence, to smooth the LCH value, an 11-order median filter was used to avoid potential sudden changes in the signal. Taking a trial of sEMG data from Dataset I as an example (details of which are described in the following section), the LCH method, LCH-Opt method, and effect of the median filtered LCH with a threshold classifier were compared. The results are shown in Fig. 5. The visual detection results, based on empirical observations, are provided by the dataset and will be detailed in the following chapter. Note that some extreme values of the LCH result, that are greater than the vertical axis upper boundary, are not displayed.
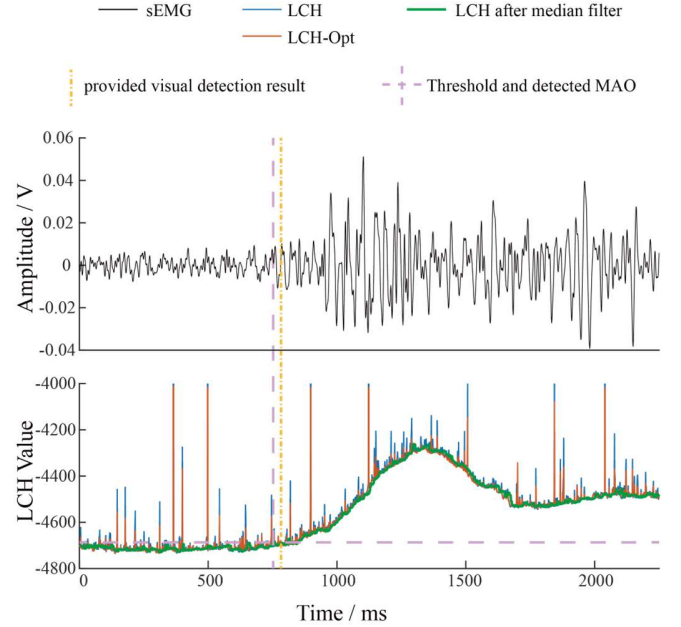
Fig. 5. Example of the proposed method for MAO detection, combining the LCH feature and only threshold (OT) classifier.

IV. EXPERIMENTAL VERIFICATION

A. Datasets Used for Validation

The MAO detection method proposed in this paper was verified on two public datasets, published by the same author in 2017 (these sEMG datasets are available online from https://github.com/TenanATC/EMG). The two datasets share the same experimental protocol and are referenced as Dataset I and Dataset II within this paper. To summarize, eighteen participants covering different ages and genders were recruited to carry out elbow flexion and knee extension tasks using their dominant limb. The subjects were seated in a stationary chair for both tasks. A 2.3 kg load was applied to the subject's ankle or wrist on the target side to improve the efficacy of the muscle contraction. Each trial was repeated three times at a
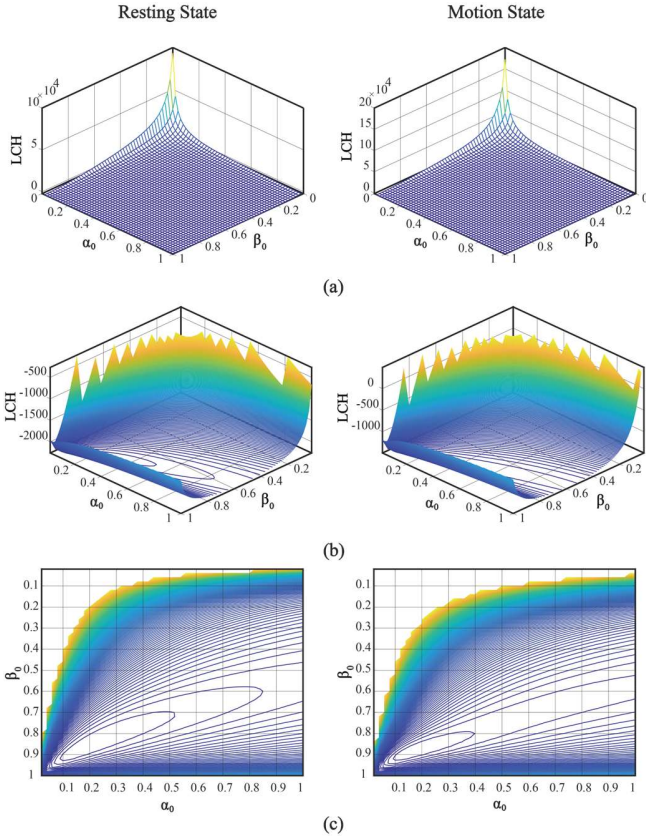

Fig. 4. Results of the LCH using different values of the parameter set, $\{\alpha_0, \beta_0\}$ in the GARCH(1,1) model. (a) Mesh plot. The step size is 0.02. (b) Contour plot. Only the values near the extreme point are retained. (c) Two-dimensional projection of the subgraph (b).

self-selected exercise pace, with at least 1 min of rest. After removing five failures, the dataset provides a total of 103 sEMG signal trials. Each trial captures a duration of approximately 3 to 5 seconds, encompassing the sEMG signals from the target muscle as it transitions from a resting to an activated state.

For the sEMG measurement, Ag/AgCl electrodes were used (B&L Engineering, Tustin, CA) with a circular diameter of 10 mm, and a 35 mm interelectrode distance. The EMG recording was characterized by the following parameters: gain 330x, >100 MΩ, 95 dB CMRR, and a 10 Hz to 3.13 kHz bandwidth. The electrodes were attached to the target muscle, determined via palpation: Biceps Brachii for elbow flexion and Vastus Lateralis for knee extension. The reference electrode was placed on the ipsilateral patella as a ground. The sEMG signals were sampled at 2048 Hz and pre-processed using a band-pass filter with a 10-1000 Hz passband. Detailed descriptions can be found in [28], [29].

The distinctive feature of this dataset is that a time value of the corresponding 'ground truth' for the onset of each muscle contraction is also provided as a benchmark. Differences in amplitude within the time domain of the signal can be visually identified by the human eye to determine the moment of muscle activation. The benchmark values were established by visual assessment on the raw sEMG signal trials, whereby three researchers labeled each trial twice within a week, so that each sEMG signal was visually inspected six times in a randomized and double-blind fashion. Hence, specifically, the study identifier and the performed movement were unknown to the assessors. The mean of the six visually appraised MAO instants was thereby adopted as a benchmark value, provided within the dataset, with which to compare different muscle activation detection methods.

Consequently, Dataset I has been broadly referenced and provides a convenient methodology for comparing the proposed MAO detection technique with other existing methods. Similarly, the method proposed in this paper was also tested on Dataset II, using the same parameters as those used for Dataset I, to demonstrate its wider efficacy.

B. Validation Content and Selected Parameters

In this implementation, the window length used was 400 sample points, corresponding to approximately 200 ms, which is a commonly used scale value in sEMG-based interfaces. The step size was set at 1 sample point, so that the LCH value would be calculated for each new sample acquisition (loaded from the Dataset) without utilizing subsequent information, which is called pseudo-online analysis. The threshold classifier was initialized using the LCH values determined from the first 200 samples, and subsequently commenced evaluating the muscle activation in pseudo-real-time. The instant in which the signal exceeded the threshold for the first time was recorded as the detection result, and the error value was obtained by comparing this with the corresponding benchmark value. For comparison, the error values from all the trials were statistically evaluated using the mean value, standard deviation (SD), median value, and interquartile range bounds—specifically, the 25th percentile (IQR-25), and 75th percentile (IQR-75).

In the following text an abbreviated notation is used to define the overall detection method: the acronym before the plus sign represents the utilized feature or preprocessing method applied to the sEMG signal, while the acronym after the plus sign represents the classifier type. To investigate the behavior of the LCH+OT method under noisy conditions, sEMG signal trials were further contaminated by various degrees of added noise. White Gaussian noise having the same length as the signal trials with a zero mean was generated using the MATLAB Communications Toolbox. After five different levels of noise were added, the signal-to-noise ratio (SNR) was conditioned to -1, -2, -5, -10, and -20 dB, respectively, hence the power of the added noise was approximately 1.25, 1.58, 3.16, 10, and 100 W, given that the power of the signal trials was 1 W. For each noise level, 20 different sequence seeds were generated by MATLAB to simulate different noise environments. The 103 trials from the dataset were then superimposed with the same 20 types of noise to achieve the target SNR. Therefore, each sEMG trial generated 20 sequences using this process. The LCH+OT and LCH-Opt+OT methods were then evaluated under the various simulated noisy conditions. The average of detected instants from the 20 sequences was saved as the detection result of one trial for a given SNR.

C. Other Methods for Comparison

Five recent studies were analyzed and have been listed for comparison.

The first of these referred studies reports the results achieved by the following five algorithms [13]: (1) a method based on the wavelet transform process and likelihood-based test statistic, WT+TS [19]; (2) a low-pass filter and only threshold technique, LPF+OT [15]; (3) a method using a TKEO preprocessor and classifier based on Bayesian change-point detection [18] with various posterior probability, TKEO+BCD [28], [29]; (4) a method based on the sum of TKEO-conditioned data points, TKEO+CUSUM, and segmented regressions (SR) finding elbow points in the scree plot, named SPE. The classifier used has many other variations, such as SPE-RefineElbow; (5) a method alternating the classifier to the profile likelihood maximization [30], TKEO+PLM. When the data distribution uses a different type of probability density function, a variation of this method is derived, such as PLM- Laplacian (PLM-Lap) and PLM-Gaussian (PLM-Gau).

The second reference study proposed a method named PROLIFIC [12]. An approach grounded on the discrete Fibonacci search method, PLM-DFS, or namely PROLIFIC was established utilizing the TKEO preprocessor and PLM method. This study also compared several variants using different probability density functions.

The third study [31] provides MAO detection results achieved by the following four algorithms: (1) threshold and post-processor, TP [17]; (2) a continuous wavelet decomposition, CWD + TP [32], or namely WT + TP; (3) the cumulative sum algorithm [14], CUSUM; (4) the PROLIFIC method proposed in the aforementioned paper [12]. The filtering procedure, ETKEO was also ascertained to be better than TKEO in this study.

The fourth referenced work [33] compares the four existing methods from the first study with a new method, WT+OT.

Specifically, an index based on the square of the absolute value of the WT coefficient and a threshold using the global information was proposed for MAO detection.

Lastly, the fifth study proposed a new method; a machine learning based, online classifier, ML, [21] and compared it with the existing four methods. The input feature combines LPF, the root mean square (RMS), and WT.

Based on the described previous investigations, the methods used for comparison in this paper were listed in Table I. The methods which demonstrated a poor performance in the previous studies were excluded from comparison in this paper, for example: (1) "general time series mean/variance, sequential and batch processing of parametric and nonparametric tools" in [28]; (2) BCD-60, BCD-95, SPE-MultiThresholdElbow, PLM-Gaussian or other distributions from [13]; (3) PLM-DFS-Lap or other distributions from [12].

V. Result

A. Comparison of Detection Methods

As an open-source dataset, various other studies have verified their methods on Dataset I and obtained results with similar evaluation indexes. The outcomes from

Several of these methods were verified on a subset of Dataset I, in which researchers selectively screened for signals with relatively high noise content via certain criteria, such as having an SNR < 8. Hence, the results from such subsets are inconsistent among studies as the calculation methods may differ. Moreover, the result of MAO detection using such a subset is likely to be relatively poor as it would be exclusively evaluated in noisy conditions.

This paper labels several of the described methods as offline methods, which would be inapplicable to EMG-based interfaces requiring real-time analysis. Here, offline methods indicate a 'noncausal system', whereby only after the complete signal trial is acquired, could such a method detect

MAO, or offset, using the comparison between the rest and motion states to optimize the sudden change. The advantage of the research described in this paper, however, is the applicability of the detection method to online applications. As such, the results are not directly compared with offline methods, in terms of the evaluation indexes, as evidently, in having the global time series data available for post-processing analysis, offline methods are often significantly more effectual.

Table I presents a comparison between detection methods. Note that these results are based on the absolute magnitude of the error, therefore, any MAO instances detected prior to the benchmark time specified in Dataset I, were assessed as errors with the same scale as MAO instances detected after the benchmark value. The results were obtained from the evaluation of the different methods on Dataset I, and the index values of the compared methods were copied from the "Result Reference". The upper section of the table presents online detection methods, while the lower section describes offline methods. In the final column labelled 'Note', a 'P' represents the use of a subset from Dataset I, and 'OFF' indicates use of an offline method. Additionally, a red background color in the numeric cells of the table indicates the comparatively best results, while a blue cell background indicates a poorer performance. This colormap is normalized for each column.

In general, the proposed LCH-based MAO detection method is superior to the existing online detection algorithms, as compared with recent studies, achieving a performance similar to the referenced offline methods. Furthermore, solely considering the online methods, the proposed technique performs best in the table based on the evaluation indexes of mean error, SD, median error, and IQR-75 values. However, the LCH detection method demonstrates a mediocre performance for the IQR-25 index. This is related to the use of an online median filter, which introduces inherent delays.

WT+ML is an improved version of WT+OT for an online

Table I. Comparison of different MAO detection algorithms assessed on the same open-source dataset (Dataset I [26]) from the perspective of five evaluation indexes: mean, standard deviation (SD), median, the upper quartile (IQR-75), and the lower quartile (IQR-25) of the errors.

Preprocessor/Feature	Classifier	Mean	SD	Median	IQR-25	IQR-75	Method Reference	Result Reference	Note
WT	TS	235	182	209	70	354	Killick et al. in 2013 [19]	TNSRE 2018 [13]	A,ON
LPF	OT	204	138	178	100	272	Hodges et al. in 1996 [15]	TNSRE 2018 [13]	A,ON
TKEO	BCD-75	115	203	39	9	119	Barry et al. in 1993 [18]	TNSRE 2018 [13]	A,ON
ETKEO	TP	134.2	203.6	69.3	31.5	146.5	Bonato et al. in 1998 [17]	TMRB 2020 [31]	P,ON
ETKEO+WT	TP	129.1	192.3	78.6	25.2	146.5	Merlo et al. in 2003 [32]	TMRB 2020 [31]	P,ON
LPF+WT+RMS	ML	92.1	120.3	54.2	13.2	93.9	Nardo et al. in 2022 [21]	SENSORS 2022 [21]	P,ON
LCH	**OT**	**65.2**	**58.1**	**44.9**	**15.9**	**98.5**	**This paper**	**This paper**	A,ON
LCH-OPT	**OT**	**55.8**	**43.3**	**50.2**	**21.4**	**77.4**	**This paper**	**This paper**	A,ON
WT	OT	34.7	61.3	10	3	27.8	Nardo et al. in 2022 [33]	ACCESS 2022 [33]	P,OFF
TKEO+CUSUM	SR	77	96	42	11	94	Selvan et al. in 2018 [13]	TNSRE 2018 [13]	A,OFF
TKEO	PLM-Lap	46	81	21	4	46	Zhu et al. in 2006 [30]	TNSRE 2018 [13]	A,OFF
TKEO	PLM-DFS-Gau	43	49	30	5	64	Suviseshamuthu et al. in 2020 [12]	ACCESS 2020 [12]	A,OFF
ETKEO+CUSUM	OT	115.5	114.8	78.6	40.3	100.3	Riedel et al. in 1994 [14]	TMRB 2020 [31]	P,OFF
ETKEO	PLM-DFS-Lap	122.2	236.1	54.9	24.9	125.5	Suviseshamuthu et al. in 2020 [12]	TMRB 2020 [31]	P,OFF

Better

Worse

P: only a part of Dataset I where trials with lower SNR was used.
A: all trials were used.

ON: online method.
OFF: offline method that is unsuitable for use in online applications.

application [21] as published recently, and demonstrates the latest in powerful methods with the help of a data-driven approach. The relative difficulty in achieving online application methods versus offline is reflected in the comparison of the tabulated results between these two different methodologies. As a preprocessing method, the use of ETKEO has greatly improved performances and, correspondingly, has been widely used. However, as highlighted in Table I, the LCH method proposed in this paper demonstrates better and more effective results than ETKEO. Only the OT classifier was applied and tested with the LCH preprocessing method due to its simplicity of implementation. Though, as with ETKEO, LCH has the potential for combination with multiple different classification methods, where other classifiers may be advantageous than OT. This should, therefore, be investigated in subsequent research.

B. Detailed Results on LCH

1) Comparison of LCH and LCH-Opt

The distribution of the MAO detection errors using the LCH and LCH-Opt methods, as evaluated on Dataset I, is shown in Fig. 6. Note that this figure illustrates the calculated error as a signed value, rather than its absolute magnitude, while the data listed in Table I provides evaluation indexes based on the absolute value of the error. Therefore, Fig. 6 highlights that the proposed MAO detection method, for some trials, generated MAO instance results ahead in time of the benchmark value provided by Dataset I, as assessed via visual inspection. These earlier detection instances may be reasonable, assuming that there is no sudden change in the signal amplitude, but the signal's internal mode may be prematurely altered which would not be detected by the investigators, but may have been extracted by the algorithm. Overlayed on the error distribution plot in Fig. 6 is a box-plot: the red line represents the mean value, and the red shaded area illustrates the 95% confidence interval of the mean. The red dotted line denotes the median value and the blue line represents the SD. These results indicate that the use of LCH-Opt narrowed the error distribution and reduced the extreme values in comparison to the LCH method. Hence, Fig. 6 indicates that the offline simplification of LCH-Opt, to the LCH method, reduces the performance.
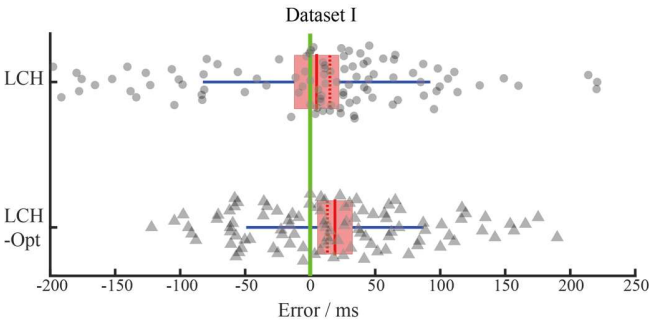

Fig. 6. Error distribution of LCH and LCH-Opt evaluated on Dataset I.

The statistical chart of LCH values is shown in Fig. 7. The solid lines and underlying shadows represent the mean and standard derivation, respectively, of all 103 trials from Dataset I. All trials were aligned on the horizontal axis by the benchmark values from Dataset I. The average LCH value before 0 s is used as the offset to normalize the curve on the

vertical axis. This operation achieves translation without scaling. Fig. 7 compares LCH and LCH-Opt and reveals that their trends are almost identical. Hence, the statistical performance of LCH is similar to that of LCH-Opt, though its variance in the resting state is slightly larger. An approximate threshold, and corresponding detection result are also shown in the figure, indicated by the dashed, horizontal, or vertical lines, respectively. The simulated threshold value was calculated by the sum of the mean and 2.5 × variance, within the initial several windows. This result verifies that online optimization improves the stability and MAO detection performance.
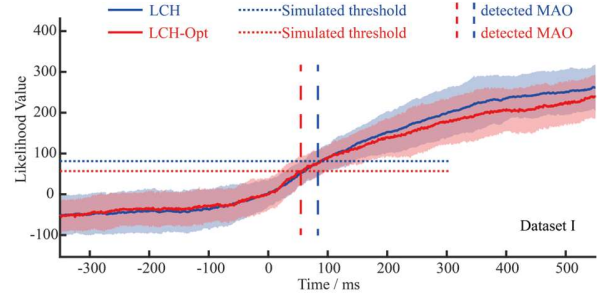

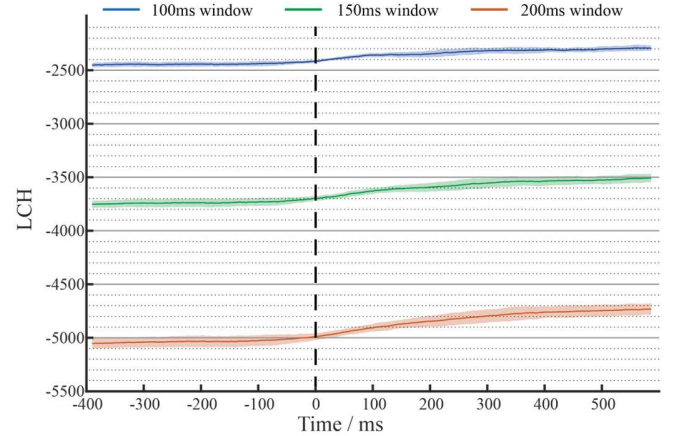Fig. 7. Statistical chart of LCH and LCH-Opt on Dataset I.

Fig. 8. Trends of LCH using different window lengths.

2) Influence of Different Parameters

Fig. 8 compares LCH values using three different window lengths applied to signals from Dataset I. It can be seen that they share the same trend. Although the longer the window length, the greater the absolute difference of LCH before and after the MAO, the relative difference remains similar. The longer the window length, the smoother the LCH, resulting in less jitter. Although most of the results in this paper were obtained with a 200 ms window length, this figure suggests that the window length has little effect on the LCH feature.

After varying the LCH window lengths to 50 ms, 100 ms, 150 ms, and 200 ms, we conducted a statistical analysis on the MAO detection errors. It was examined that the data distribution does not satisfy normality ($p = 0.001$) and homogeneity of variance ($p = 0.000$). Therefore, the nonparametric Friedman's test was conducted and produced a p-value of 0.14, suggesting that the window length does not significantly influence the MAO detection performance when using LCH. Additionally, upon conducting multiple

comparisons and paired t-tests between any two groups, no significant differences were observed. For instance, the comparison between the 50 ms and 200 ms groups yielded a p-value of 0.65. For real-time application contexts, the window length can be tailored based on the signal sampling rate or other specific needs without compromising the efficacy of the selected features and methodologies.

The scaler k value in OT is usually set based on experience. Several k values were evaluated, and the corresponding results are shown in Fig. 9. It can be seen that 4.5 is the proper k value and is consistent within the expected range of 3 to 15. The quantitative results using a k value of 4.5 are consistent with that of the LCH results shown in Table I.
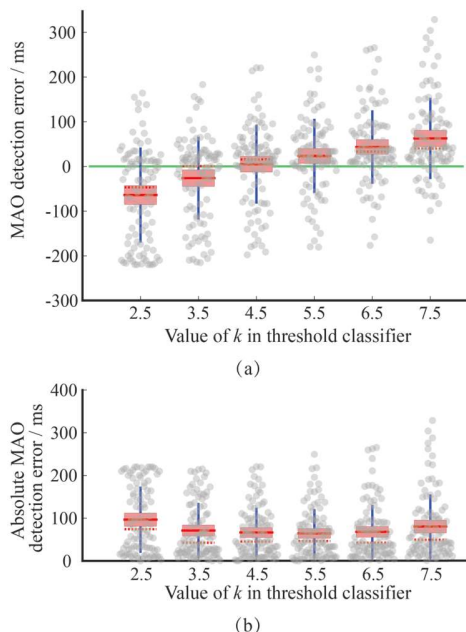

(a)

(b)

Fig. 9. Effect of k value in the threshold classifier on the MAO detection error. (a) Error distribution. (b) Absolute error distribution.

3) Calculation Consumption

Based on Eq. (13), the LCH computation entails a cumulative sum operation, with the overall computation related to the window length. When tested on an older laptop equipped with a 1.6 GHz Intel i5-8250U CPU and operating within a Matlab script environment, the computation times for window lengths of 60, 80, 100, 200, and 400 sample points were approximately 0.18, 0.35, 0.57, 2.0, and 7.2 ms, respectively. This data can be modeled by a quadratic function $y = 0.0004x^2 + 0.0019x - 0.0345$, resulting in an R2 value of 0.9999. Thus, in terms of window length n, the algorithmic complexity can be represented as $O(n^2)$. Another evaluation was conducted on an embedded controller with a 1.7 GHz CPU, operating under a C++ programming environment and achieving a real-time control frequency of 1000 Hz. The real-time operation system cannot accommodate algorithms with computation durations exceeding 1 ms. For LCH window lengths of 60, 80, and 100 sample points, the control algorithm's computation times were approximately 0.27, 0.49, and 0.72 ms. While the computational burden of LCH-Opt is notably higher than that of LCH, it is not the primary concern for the online applications discussed in this paper. Even

though LCH has a greater computational consumption compared to others, its computation duration remains within the microsecond range, rendering it apt for online applications. Given the balance between enhanced accuracy and minimized detection latency, the computational demand is considered justifiable.

4) Noise Insensitivity

After adding several levels of pseudo-random Gaussian white noise to the signals from Dataset I, the errors of MAO detection via the LCH-based method are presented in Fig. 10. Orange shading in the extreme right of the horizontal axis represents samples with an onset detection delay exceeding 250ms, which was considered as a failure. A significant difference only exists between the levels with no added noise and those with an SNR of -20 dB (p=0.02) when evaluated by a paired student's t-test.
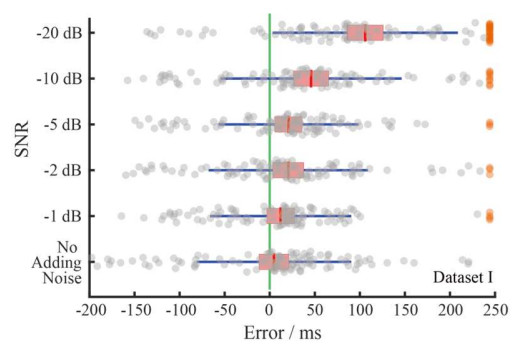

Fig. 10. Effect of additional noise on the LCH-based MAO detection method.

Fig. 11 shows the trend of LCH after adding noise. Since there are five levels of noise with 20 types of random seed, the LCH curve is double averaged from 5×20 samples and then counted from 103 trials in Dataset I. Therefore, its mean value is smoother, but not robust, and its variance is smaller, but without specific meaning. This graph reflects the influence of noise on the mean value, in that the noise reduces the absolute difference of LCH between the resting state and motion state, but does not overly affect the trend. The impact of noise on LCH-Opt has not yet been tested due to the requirement for large-capacity computing. According to Fig. 10 and Fig. 11, additional noise has little impact on the LCH feature and detection result, indicating that LCH possesses a strong anti-noise capability.

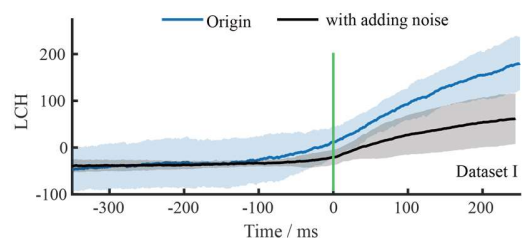
Fig. 11. Effect of additional noise on the LCH value.

C. Validation Results on the Dataset II

All the previously described experimental verification measures were also conducted on Dataset II. There was no parameter optimization, such as for window length and k value in the OT, but the LCH method performance was better, reflecting that the signal quality of Dataset II itself is superior.

A merged figure with all the results of the tests on Dataset II is provided as Fig. 12, though no further description, or analysis will be given in detail.

VI. Discussion

A. Universality of the Method

Some previous research spliced data from resting and motion states to simulate sEMG signals [13], [28] where there is a sudden change in amplitude, indicating a change in muscle activation state. However, such data is considered of little meaning as the recruitment of motor units is a gradual process rather than an abrupt change. The foundation of MAO

Fig. 12. Results of the experimental verification measures on Dataset II. (a) Error distribution of LCH and LCH-Opt. (b) Statistical chart of LCH and LCH-Opt. (c) Effect of additional noise on LCH-based MAO detection. (d) Effect of additional noise on LCH.

detection should be in extracting information from the signal that indicates the start of a neural impulse firing and subsequent recruitment of motor units. Such detailed signal features may be absent in spliced data.

As discussed in Section II, only two segments of an sEMG trial were used to form the model analysis. However, Dataset I which was used to validate this method, has samples in various conditions, so its results can demonstrate the wider dependability of this method. Specifically, it contains data from two distinct motor tasks using different muscles, where subjects moved the corresponding joint at a voluntary speed. Therefore, the recorded sEMG trials exhibit different SNRs, ranging from approximately 1.6 to 27 dB. Hence, LCH, as an offline optimized version of LCH-Opt, demonstrates universality, and the parameter set $\{0,0.1,0.9\}$, represents the general conditions of the GARCH model for modelling a surface EMG signal. The results of the LCH method on Dataset I were acquired after a simple optimization of the k value used in the threshold classifier.

When the proposed method was validated on Dataset II with identical model parameters, the effect was improved, outdoing the results from Dataset I. This indicates that all parameters, including the k value, are not the result of over-fitting, and that the proposed method has capability for generalization across different datasets.

B. Model Properties

The full GARCH model has many properties and constraints. The boundedness constraint, $\alpha_0 + \beta_0 < 1$, was ignored in this research. As the model will not be used for long-term predictions, the stability of the model was considered less important. Thus, these parameter constraints are ignored in the LCH-Opt and offline determination of model parameters, however, this does not affect its performance for MAO detection. Additionally, the parameter set is not necessarily restricted to the quoted values of $\{0,0.1,0.9\}$. Other parameter value sets, around the extreme value, were established as having the same results, for example, the value set $\{0,0.2,0.85\}$.

LCH-Opt is equivalent to the LCH method, but uses parameter values found through the online identification of the GARCH model. Its value sequence is always smoother than that of the LCH method, having less noise. However, to improve the real-time performance, the online optimization process is omitted in the proposed LCH method, and instead a median filter is introduced to ensure the same effect. Another improvement on the LCH method is to remove the second term in Eq. (13), and only accumulate the logarithmic value of the variance, where the median filter can then be omitted. This is because the second term of the LCH calculation, comprising of a division operation, may easily amplify the error and thereby, generate additional noise.

From the perspective of real-time performance, a shorter window length is beneficial for discarding historical information and updating the motion state, as well as reducing computational load. Therefore, even with the slightly longer window length of 200 ms used in Section V.A, satisfactory accuracy results can still be achieved, reflecting the effectiveness of the method.
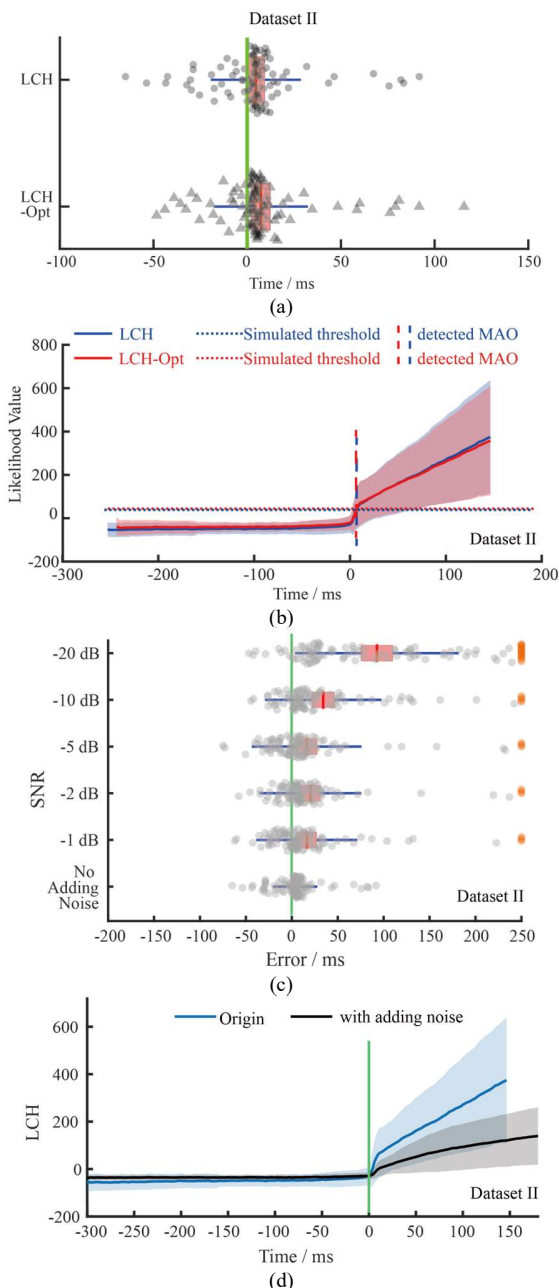
The proposed LCH method performs mediocrely on the IQR-25 evaluation index, which is likely to be related to the inherent delay of online median filtering. As illustrated in Fig. 6, the MAO detection results of this method generally provide an onset instance value earlier than the benchmark time determined by visual detection, thereby leading to an increase in the mean absolute error. While this may be because the threshold is low, and thus is wrongly detecting the onset prematurely within the rest state. It is certainly also possible that the true muscle activation onset instance may be earlier than is discernable by visual detection, particularly in any trials with low SNR. Although the signal may not exhibit a sudden change in amplitude, the difference in its intrinsic pattern is extracted by the algorithm, which may be enabling an earlier detection of muscle activation.

As shown in Fig. 10, LCH was demonstrated as being relatively insensitive to noise. Two potential reasons for this are speculated: This method was developed to model the signal variance rather than the amplitude, so the amplitude, or power, of the noise has less influence on the MAO detection. Alternatively, according to Eq. (1) and (3), the innovation and error are viewed as white Gaussian noise. Additional white noise may have little effect on the absolute difference in LCH between the resting state and motion state, but will reduce its relative difference. Correspondingly, previous research has also revealed that the AR-GARCH model is insensitive to data noise[34]. The specific mechanism and impact may warrant further analysis.

GARCH has also been used for signal segmentation in previous studies [35], for example, in methods based on test statistics [36] and the conditional variance [24], which are distinct methods from those discussed in this paper. This suggests that GARCH has a strong applicability for use in change point detection due to its usage in separate methods, emanating from different foundational work.

C. Limitations and Future Work

Eq. (13) shows that LCH is a cumulative sum of values from all windowed samples. Although it can be used in online applications, it demands greater computational effort than other methods, such as TKEO and LPF. Algorithms for providing additional enhancements need further research. It is found that if fixed AR coefficients (offline calculated from resting state) were used in pseudo-online MAO detection, the difference of LCH in resting and motion states will be widened.

Although LCH is termed a feature in this paper, it can only be applied to MAO detection at present. The feasibility of this feature for a multi-classification task, such as gesture recognition, needs further investigation.

The experimental verification process used in this paper is equivalent to pseudo-online analysis of datasets. In the future, the proposed method will be applied to the online control of an exoskeleton as a supplement to a physical HMI. While this method is also useful for offset detection and signal segmentation, as an HMI, it is best tuned to the detection of muscle activation onset with low latency requirements.

The classifier type used alongside the LCH method was not investigated or compared in this paper. A basic threshold classifier, without adaptation, was utilized due to the simplicity and convenience of its implementation. The results of the LCH method in Table I may be further improved by also optimizing the classifier. A simple optimization could revise the TP by using a double threshold [17] or some form of post-processor. Hence, future research could focus on the exploration and application of alternative classifiers, such as BCD, PLM, or learning-based models such as temporal convolutional networks.

VII. Conclusion

This paper introduces a novel feature, LCH, for online muscle activation detection. Firstly, this paper analyzes and models sEMG signals based on the AR-GARCH model. Due to the existence of heteroskedasticity in the motion state, and recognition of its absence in the resting state, it was found that the likelihood of parameters of the GARCH model were different in the process of maximum likelihood estimation. Therefore, the described LCH-Opt method is proposed as a preprocessing feature for MAO detection. To simplify the calculations, the online model parameter estimation may be replaced by a fixed parameter set, and thus, the LCH method is subsequently derived. The proposed preprocessing feature, used in combination with a threshold classifier, was validated on two public sEMG datasets, and the corresponding results were directly compared with several other methods from previous research. As an online detection method, the MAO detection accuracy of this technique demonstrated an excellent performance compared to existing online methods. Additionally, the LCH method provides a further advantage in its insensitivity to noise. In summary, this paper provides results for the proposed LCH feature used for MAO detection and evaluated on experimental sEMG data, which demonstrates its strong applicability for use in online signal detection or segmentation, and corresponding future research.

Appendix: Abbreviations

The acronyms used in this paper are listed in Table II.

References

[1] D. Farina *et al.*, "The extraction of neural information from the surface EMG for the control of upper-limb prostheses: Emerging avenues and challenges," *IEEE Trans. Neural Syst. Rehabil. Eng.*, vol. 22, no. 4, pp. 797–809, 2014.

[2] M. del Olmo and R. Domingo, "EMG characterization and processing in production engineering," *Materials (Basel).*, vol. 13, no. 24, pp. 1–28, 2020.

[3] I. L. Petersen, W. Nowakowska, C. Ulrich, and L. N. S. A. Struijk, "A novel sEMG triggered FES-hybrid robotic lower limb rehabilitation system for stroke patients," *IEEE Trans. Med. Robot. Bionics*, vol. 2, no. 4, pp. 631–638, 2020.

[4] D. Hollinger, M. Schall, H. Chen, S. Bass, and M. Zabala, "The influence of fait phase on predicting lower-limb joint angles," *IEEE Trans. Med. Robot. Bionics*, vol. 5, no. 2, pp. 343–352, 2023.

[5] Y. Xu, D. Zhang, Y. Wang, J. Feng, and W. Xu, "Two ways to improve myoelectric control for a transhumeral amputee after targeted muscle reinnervation : a case study," pp. 1–11, 2018.

[6] F. Gasparic *et al.*, "Nonlinear Mapping From EMG to Prosthesis Closing Velocity Improves Force Control With EMG Biofeedback," *IEEE Trans. Haptics*, vol. 16, no. 3, pp. 379–390, Jul. 2023.

[7] R. Yang, Z. Shen, Y. Lyu, Y. Zhuang, L. Li, and R. Song, "Voluntary Assist-as-Needed Controller for an Ankle Power-Assist Rehabilitation Robot," *IEEE Trans. Biomed. Eng.*, vol. 70, no. 6, pp. 1795–1803, Jun. 2023.

[8] T. Proietti, E. Ambrosini, A. Pedrocchi, and S. Micera, "Wearable robotics for impaired upper-limb assistance and rehabilitation: state of the art and future perspectives," *IEEE Access*, vol. 10, pp. 106117–106134, 2022.

[9] E. S. Page, "Continuous Inspection Schemes," *Biometrika*, vol. 41, no. 1/2, pp. 100–115, Jun. 1954.

[10] B. Namoano, A. Starr, C. Emmanouilidis, and R. C. Cristobal, "Online change detection techniques in time series: An overview," in *2019 IEEE International Conference on Prognostics and Health Management*, Jun. 2019, pp. 1–10. doi: 10.1109/ICPHM.2019.8819394.

[11] C. Truong, L. Oudre, and N. Vayatis, "Selective review of offline change point detection methods," *Signal Processing*, vol. 167, p. 107299, 2020.

[12] E. S. Suviseshamuthu, D. Allexandre, U. Amato, B. Della Vecchia, and G. H. Yu, "PROLIFIC: A fast and robust profile-likelihood-based muscle onset detection in electromyogram using discrete fibonacci search," *IEEE Access*, vol. 8, pp. 105362–105375, 2020.

[13] S. E. Selvan, D. Allexandre, U. Amato, and G. H. Yue, "Unsupervised stochastic strategies for robust detection of muscle activation onsets in surface electromyogram," *IEEE Trans. Neural Syst. Rehabil. Eng.*, vol. 26, no. 6, pp. 1279–1291, 2018.

[14] K. S. Riedel, M. Basseville, I. V. Nikiforov, and M. Basseville, *Detection of Abrupt Changes: Theory and Application*. 1994. doi: 10.2307/1269388.

[15] P. W. Hodges and B. H. Bui, "A comparison of computer-based methods for the determination of onset of muscle contraction using electromyography," *Electroencephalogr. Clin. Neurophysiol. - Electromyogr. Mot. Control*, vol. 101, no. 6, pp. 511–519, 1996.

[16] J. F. Kaiser, "On Teager's energy algorithm and its generalization to continuous signals," in *4th IEEE Digital Signal Processing Workshop*, 1990, pp. 2–3.

[17] P. Bonato, T. D'Alessio, and M. Knaflitz, "A statistical method for the measurement of muscle activation intervals from surface myoelectric signal during gait," *IEEE Trans. Biomed. Eng.*, vol. 45, no. 3, pp. 287–299, 1998.

[18] D. Barry and J. A. Hartigan, "A Bayesian analysis for change point problems," *J. Am. Stat. Assoc.*, vol. 88, no. 421, pp. 309–319, Mar. 1993.

[19] R. Killick, I. A. Eckley, and P. Jonathan, "A wavelet-based approach for detecting changes in second order structure within nonstationary time series," *Electron. J. Stat.*, vol. 7, no. 1, pp. 1167–1183, 2013.

[20] J. Liu, D. Ying, W. Z. Rymer, and P. Zhou, "Robust muscle activity onset detection using an unsupervised electromyogram learning framework," *PLoS One*, vol. 10, no. 6, p. e0127990, 2015.

[21] F. Di Nardo, A. Nocera, A. Cucchiarelli, S. Fioretti, and C. Morbidoni, "Machine learning for detection of muscular activity from surface EMG signals," *Sensors*, vol. 22, no. 9, p. e3393, Apr. 2022.

[22] E. Trigili *et al.*, "Detection of movement onset using EMG signals for upper-limb exoskeletons in reaching tasks," *J. Neuroeng. Rehabil.*, vol. 16, no. 1, pp. 1–16, Dec. 2019.

[23] R. F. Engle, "Autoregressive Conditional Heteroscedasticity with Estimates of the Variance of United Kingdom Inflation," *Econometrica*, vol. 50, no. 4, pp. 987–1007, Jul. 1982.

[24] G. Rasool, N. Bouaynaya, and K. Iqbal, "Muscle activity detection from myoelectric signals based on the AR-GARCH model," in *2012 IEEE Statistical Signal Processing Workshop (SSP)*, Aug. 2012, pp. 420–423. doi: 10.1109/SSP.2012.6319721.

[25] G. Rasool, N. Bouaynaya, K. Iqbal, and G. White, "Surface myoelectric signal classification using the AR-GARCH model," *Biomed. Signal Process. Control*, vol. 13, no. 1, pp. 327–336, 2014.

[26] R. J. Triolo, D. H. Nash, and G. D. Moskowitz, "The identification of time series models of lower extremity EMG for the control of prostheses using Box-Jenkins criteria," *IEEE Trans. Biomed. Eng.*, vol. 35, no. 8, pp. 584–594, 1988.

[27] K. Mukherjee, "M-estimation in GARCH models," *Econom. Theory*, vol. 24, no. 6, pp. 1530–1553, 2008.

[28] M. S. Tenan, A. J. Tweedell, and C. A. Haynes, "Analysis of statistical and standard algorithms for detecting muscle onset with surface electromyography," *PLoS One*, vol. 12, no. 5, p. e0177312, 2017.

[29] M. S. Tenan, A. J. Tweedell, and C. A. Haynes, "Iterative assessment of statistically-oriented and standard algorithms for determining muscle onset with intramuscular electromyography," *J. Appl. Biomech.*, vol. 33, no. 6, pp. 464–468, 2017.

[30] M. Zhu and A. Ghodsi, "Automatic dimensionality selection from the scree plot via the use of profile likelihood," *Comput. Stat. Data Anal.*, vol. 51, no. 2, pp. 918–930, 2006.

[31] A. Tigrini, A. Mengarelli, S. Cardarelli, S. Fioretti, and F. Verdini, "Improving EMG signal change point detection for low SNR by using extended Teager-Kaiser energy operator," *IEEE Trans. Med. Robot. Bionics*, vol. 2, no. 4, pp. 661–669, 2020.

[32] A. Merlo, D. Farina, and R. Merletti, "A fast and reliable technique for muscle activity detection from surface EMG signals," *IEEE Trans. Biomed. Eng.*, vol. 50, no. 3, pp. 316–323, 2003.

[33] F. Di Nardo, T. Basili, S. Meletani, and D. Scaradozzi, "Wavelet-based assessment of the muscle-activation frequency range by EMG analysis," *IEEE Access*, vol. 10, pp. 9793–9805, 2022.

[34] S. Y. Sohn and M. Lim, "Hierarchical forecasting based on AR-GARCH model in a coherent structure," *Eur. J. Oper. Res.*, vol. 176, no. 2, pp. 1033–1040, 2007.

[35] S. Mousazadeh and I. Cohen, "AR-GARCH in presence of noise: Parameter estimation and its application to voice activity detection," *IEEE Trans. Audio, Speech Lang. Process.*, vol. 19, no. 4, pp. 916–926, 2011.

[36] R. Tahmasbi and S. Rezaei, "Change point detection in GARCH models for voice activity detection," *IEEE Trans. Audio, Speech Lang. Process.*, vol. 16, no. 5, pp. 1038–1046, 2008.